



CZTS counter electrode in dye-sensitized solar cell: enhancement in photo conversion efficiency with morphology of TiO₂ nanostructured thin films

Jitendra P. Sawant¹ · Rohidas B. Kale¹

Received: 20 June 2019 / Revised: 14 November 2019 / Accepted: 15 November 2019 / Published online: 25 November 2019
© Springer-Verlag GmbH Germany, part of Springer Nature 2019

Abstract

In the present investigation, kesterite phase Cu₂ZnSnS₄ (CZTS) nanoparticle, and one-dimensional (1D) nanorods and three-dimensional (3D) flower-like rutile phase TiO₂ thin films were obtained by the conventional hydrothermal method. The (112) plane-oriented single-phase CZTS nanoparticles with chemical composition Cu/(Zn + Sn) = 0.84, 0.90, 1.05 were obtained by changing the copper concentration of the precursor solution. The CZTS thin films were prepared on fluorine-doped tin oxide (FTO) substrate by the doctor blade coating method. The effect of reaction time on growth of the hydrothermal deposited rutile phase TiO₂ nanorod thin films were investigated. The detailed structural properties, phase identification, and morphological developments were investigated using X-ray diffraction (XRD), Raman spectroscopy, high-resolution transmission electron microscopy (HRTEM), and scanning electron microscopy (SEM) techniques. The dye-sensitized solar cells were fabricated with CZTS counter electrodes (CEs) and hydrothermal deposited nanostructured TiO₂ photoanodes. The device formed with three-dimensional TiO₂ nanostructured photoanode showed higher efficiency (2.65%) than one-dimensional microstructures (1.74%). The study demonstrates that the nanostructure-based morphologies of TiO₂ photoanodes affect the performance of CZTS CE-based dye-sensitized solar cell.

Keywords CZTS nanoparticles · TiO₂ nanostructures · DSSC counter electrode · 2.65% efficiency

Introduction

The Cu₂ZnSnS₄ (CZTS), a kesterite phase semiconductor, has been attracting a lot of attention, for the development of new generation photovoltaic devices. It is a high-quality semiconductor, consists of cheap, earth-abundant, nontoxic elements such as Cu, Zn, Sn, and S [1, 2]. The CZTS exhibits an excellent light absorption coefficient about $\geq 10^4$ cm⁻¹ [3, 4], direct energy band gap (E_g) ~ 1.45–1.6 eV, which is close to the optimum value for being used as an efficient light-absorbing layer in the thin film solar cells [2, 5]. Owing to the excellent properties, CZTS considered as a promising material and explored in different types of solar cell

configurations such as thin film solar cells [6–8], dye-sensitized solar cell (DSSCs) [9–11], quantum dot DSSCs [12, 13], and perovskite [14, 15] solar cell configurations.

Dye-sensitized solar cells (DSSCs), because of low-cost and easy fabrication process, have attracted much attention. The counter electrodes (CEs) are the most important component of DSSCs, which catalyzes the reduction of redox electrolyte by collecting photo-generated free electrons from the external circuit. The synthesis method and elemental compositions as well as morphology of CZTS CEs [10, 11] play a vital role in the performance of CZTS-based DSSCs. A solvothermal synthesized CZTS CE on FTO (fluorine-doped tin oxide, SnO₂: F) substrate showed an efficiency of 5.65% [16]. Kong et al. [17] used wurtzite and kesterite phase CZTS nanocrystalline thin films as CEs and demonstrated wurtzite CZTS as a superior CE (6.23%) than kesterite phase CZTS CE (4.89%). Chen et al. [10] employed nanoleaf-like plates of CZTS CEs (solvothermal treatment on electrodeposited CuZnSn films) in dye-sensitized solar cell and reported 8.67%, which is the highest efficiency so far with CZTS-

Dedicated to the memory of Ivo Alexandre Hümmelgen

✉ Jitendra P. Sawant
jitendrasawant34@gmail.com

¹ Department of Physics, The Institute of Science, 15 Madam Cama Road, Fort, Mumbai 400032, India

based counter electrodes. A wide band gap semiconductor TiO_2 is a most promising and widely used photoanode in dye-sensitized solar cell [18]. The crystalline TiO_2 has three polymorphic forms such as anatase ($E_g = 3.23$ eV), a more stable rutile ($E_g = 3.02$ eV) and brookite [19]. Dye-sensitized solar cell has shown higher power conversion efficiency with a large surface area of TiO_2 photoanodes [20]. The mobility of carriers in TiO_2 as a photoanode is strongly dependent on the morphology [18, 21]. A highly oriented one-dimensional nanorods and nanotubes structured array of TiO_2 photoanode have shown excellent photovoltaic efficiency in dye-sensitized solar cell [22–24].

A variety of physical and chemical methods have been studied and explored to synthesize different structures of CZTS. Which mainly includes chemical vapor deposition, thermal evaporation, sputtering, electrodeposition, and spray pyrolysis. [25–29]. However, the conventional solution processes for synthesis of CZTS nanoparticles are low-cost and competitive techniques, which yield better phase and composition control of the compounds [27, 30]. Solvothermal and hydrothermal methods have employed to form high-quality CZTS nanoparticles [31–33]. The green, reliable, and nontoxic solvent-based solution process for CZTS synthesis is always favorable for large-scale production of CZTS-based solar cell [34]. Among them, hydrothermal method is low cost, environmental friendly, and suitable for large-scale synthesis of high-quality nanoparticles.

In the present work, we report on the hydrothermal synthesis of CZTS nanoparticles. The CZTS thin films were deposited on FTO substrate using the doctor blade coating method. One-dimensional (1D) compact nanorods and three-dimensional (3D) microflowers of TiO_2 nanostructured thin films were grown on FTO substrate using the hydrothermal technique. The TiO_2 films as a photoanode were loaded with N719 dye and tested with CZTS as a counter electrode for the DSSCs performance.

Experimental

Materials

Cupric sulfate pentahydrate ($\text{CuSO}_4 \cdot 5\text{H}_2\text{O}$), zinc sulfate ($\text{ZnSO}_4 \cdot 7\text{H}_2\text{O}$), stannous chloride ($\text{SnCl}_2 \cdot 2\text{H}_2\text{O}$), thiourea ($(\text{NH}_2)_2\text{CS}$), TTIP, (36%) HCl, ethyl cellulose, terpineol, ethanol, and N719 dye [di-tetrabutylammoniumcis-bis(isothiocyanato) bis(2,2'-bipyridyl-4,4'-dicarboxylato)] were purchased from S.D. Chem. Ltd. and used without further purification.

Deposition of CZTS thin film as a counter electrode

CZTS nanoparticles were synthesized using the hydrothermal method. In a typical synthesis, (0.005 M) $\text{CuSO}_4 \cdot 5\text{H}_2\text{O}$,

(0.005 M) $\text{ZnSO}_4 \cdot 7\text{H}_2\text{O}$, (0.005 M) $\text{SnCl}_2 \cdot 2\text{H}_2\text{O}$, and 0.05 M thiourea were dissolved in water. The resultant solution stirred for half an hour and transferred into Teflon-lined stainless steel autoclave. The autoclave filled with 75% of its capacity and kept in hot air oven for 24 h at 180 °C. After that, the oven allowed for cooling naturally to room temperature. The black-colored product was collected and washed with distilled water and ethanol several times and dried at 80 °C for 10 h. Three samples were obtained with 0.005, 0.01, and 0.015 M of copper concentrations, and corresponding samples were named as C1, C2, and C3 respectively. After that, 10 mg of CZTS sample (C2) and 3 mg of ethyl cellulose were mixed together. A premixed solution of ethanol and of terpineol (10:1) added dropwise in the mixture containing CZTS and ethyl cellulose to form a suitable viscous CZTS paste. The resulted paste then coated on an ultrasonic-cleaned FTO substrate and annealed at 250 °C for 30 min. The CZTS/FTO thin films were used as a counter electrode to study the performance of the dye-sensitized solar cell. The schematic representation of the mechanism of hydrothermal synthesized CZTS nanoparticles and the doctor blade coating of CZTS thin films is shown in Fig. 1.

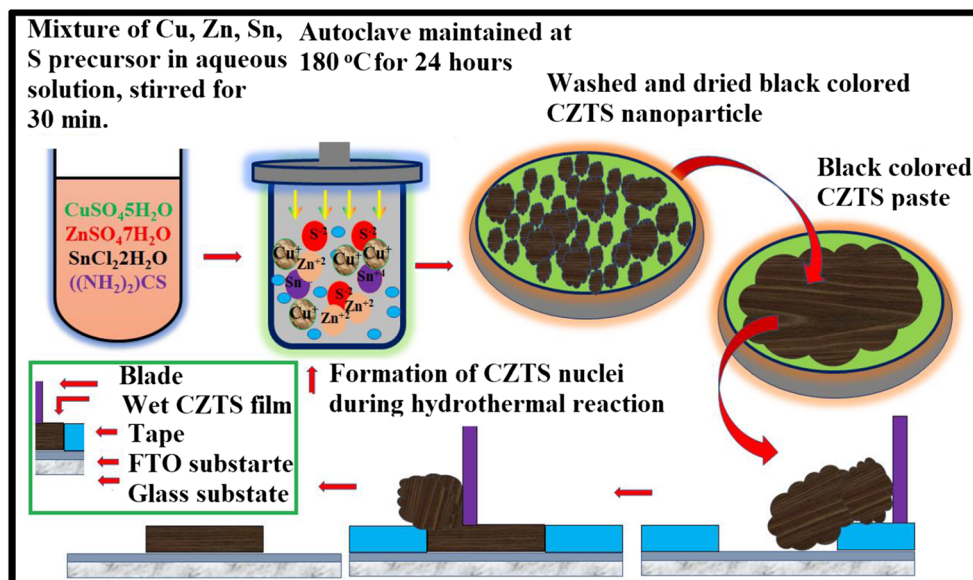
Deposition of TiO_2 nanorods as a working electrode

TiO_2 nanostructured thin films were deposited on FTO glass substrate using the hydrothermal method. In deposition process, 1 ml of titanium isopropoxide dissolved in equal volume of distilled water and HCL (36%) by stirring for 30 min. The mixture then transferred into Teflon-lined stainless steel autoclave. The cleaned FTO substrate placed in autoclave facing the conducting surface sliding down against the wall of the container. The autoclave then maintained at 180 °C and the kept for 3, 5 and 7 h. Autoclave then allowed to cool naturally to room temperature and thin films containing TiO_2 nanorods were collected. The films were rinsed with distilled water several times to remove loosely bonded surface molecules and dried naturally. The dried samples annealed at 400 °C for 1 h and used for further characterizations. The film deposited at 3, 5, and 7 h of deposition time were named as A1, A2, and A3 respectively. Figure 2 shows the schematics of hydrothermal synthesis of nanostructured TiO_2 thin film.

Fabrication of solar cell device

The CZTS/FTO was employed as a counter electrode in DSSC device. Hydrothermal deposited TiO_2 thin films were placed in ethanolic solution of 0.5 mM N719 dye for 24 h and used as a photoelectrode. The CZTS/FTO counter electrodes facing the TiO_2 photoelectrode held together using binder clip on opposite end. Just before the analysis, drops of electrolyte containing 0.5 M LiI, 0.05 M I_2 , and 0.5 M tetrabutyl pyridine induced in sandwiched cell until no air bubble is present. The light falls on the back contact of FTO and penetrates the dye adsorbed onto the

Fig. 1 Schematic representation of formation mechanism of CZTS nanoparticles and doctor blade coating of CZTS thin film



TiO₂ photoelectrode. Figure 3 depicts the schematic representation of CZTS counter electrode and N719-TiO₂ working electrode in dye-sensitized solar cell with a possible electron transport mechanism.

Characterizations

The structural and phase determination was carried out using X-ray diffraction (XRD) measurements (model XPERT-PROMPD spectrometer) with CuK_α radiation of wavelength 1.5410 Å. Raman spectrum was recorded using a Raman spectrometer in the range 600–2100 cm⁻¹ and excitation source having wavelength 532 nm of He-Ne laser. The scanning electron microscopy (SEM, JEOL JSM-IT300) and high-resolution transmission

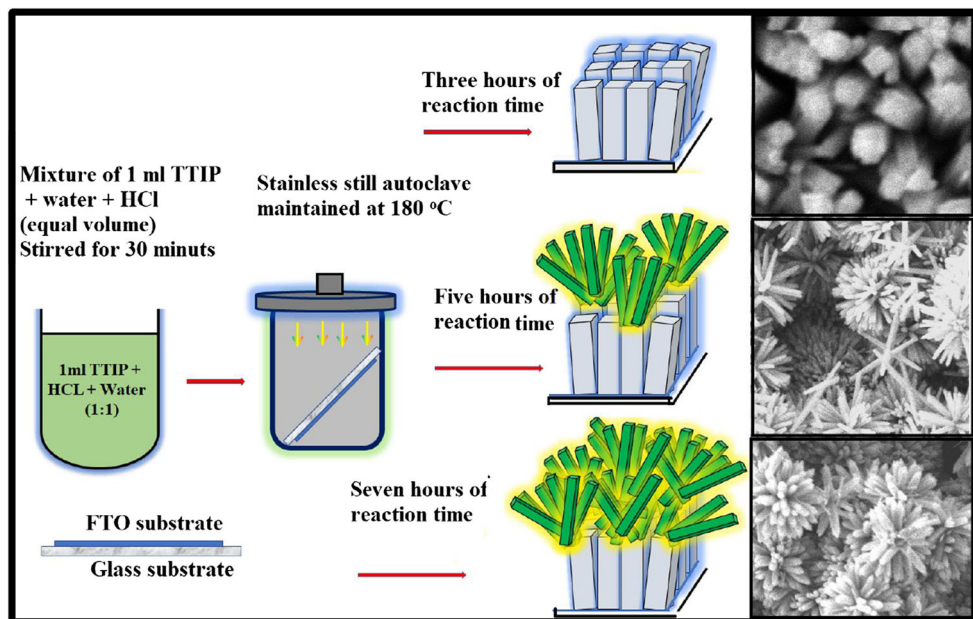
electron microscopy (HRTEM, JEOL JEM-2100F, 200 kV) were used for morphological study. The optical absorption spectra were recorded using a UV-vis spectrometer (Perkin Elmer). The fabricated DSSC device was tested for *I*-*V* characteristics under an air mass (AM) of 1.5 global (AM 1.5 G) conditions with a solar simulator (100 mW/cm²).

Results and discussion

Morphology and compositional analysis

Figure 4 a–f show morphological features of CZTS nanoparticles synthesized using different copper concentration. At

Fig. 2 Schematic representation of the formation of nanostructured TiO₂ thin films by hydrothermal method



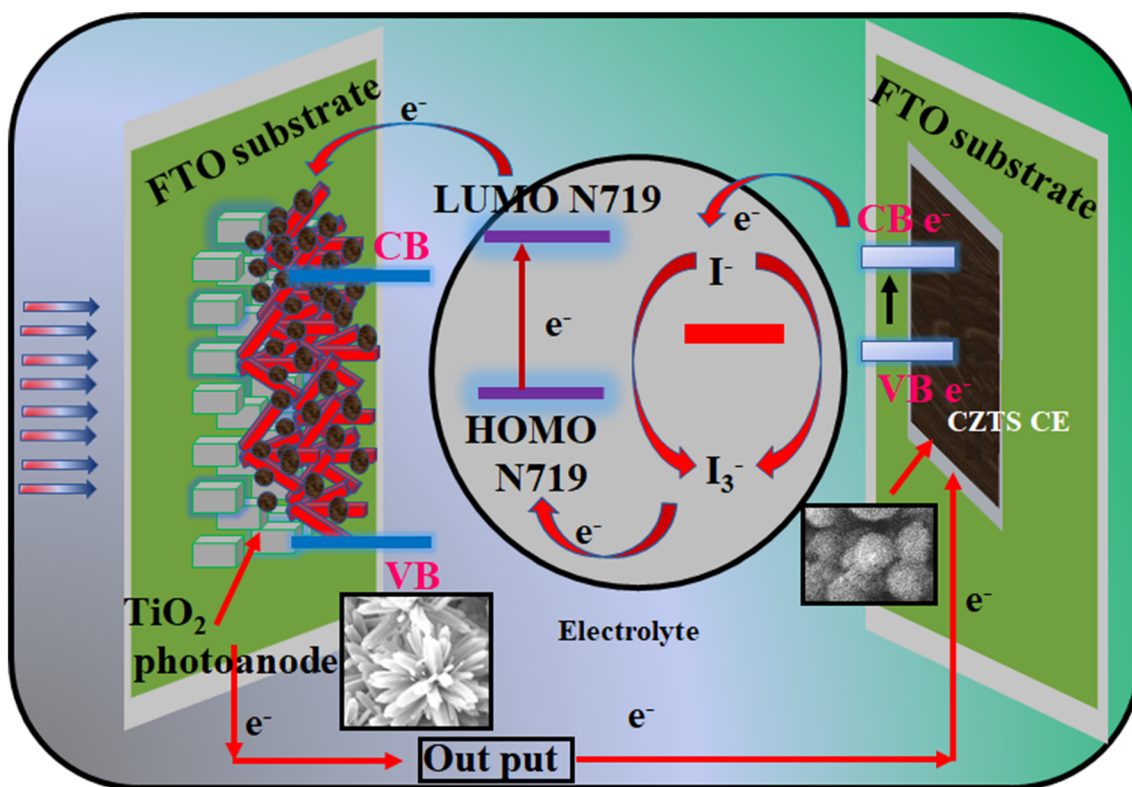


Fig. 3 Schematic representation of DSSCs employing CZTS counter electrode and N719-TiO₂ working electrode with possible electron transport mechanism

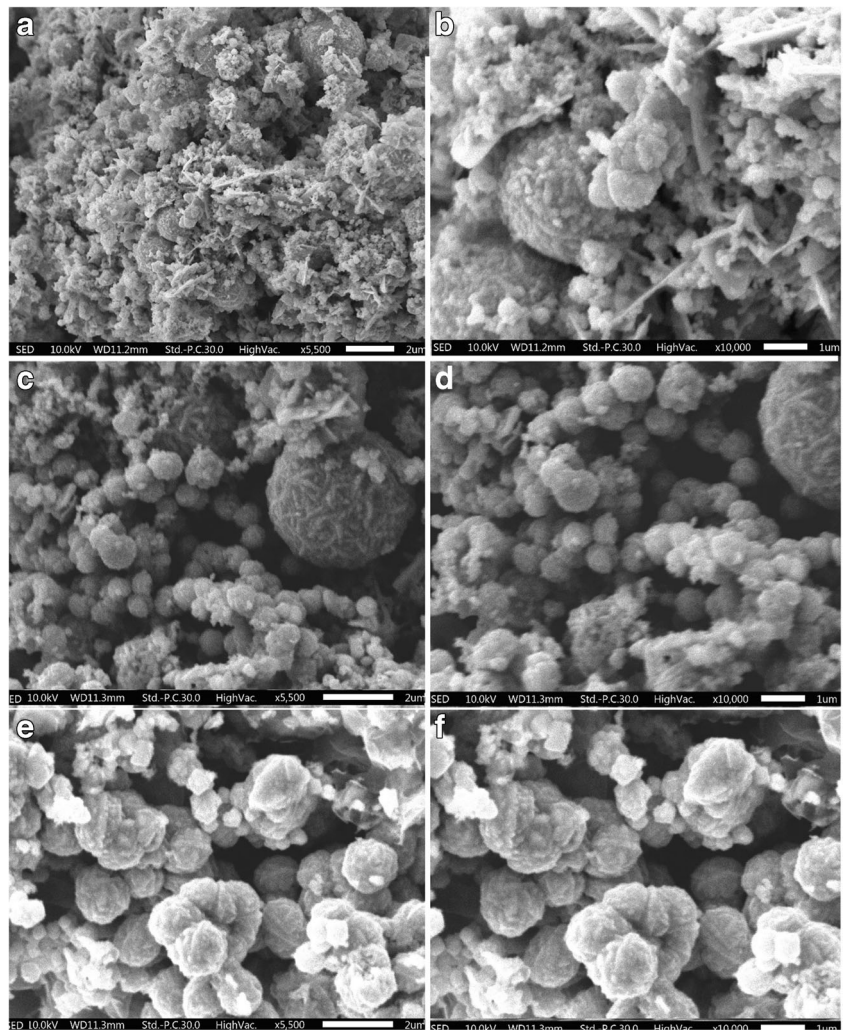
lower copper concentration, general morphologies of CZTS nanoparticles were observed (sample C1, Fig. 4a, b). As Cu concentration in the precursor solution increased, the particle starts to aggregate and converted into compact, solid microspheres of around $\sim 1\text{--}3\ \mu\text{m}$ diameters (Fig. 4c, d). The CZTS synthesized at a higher copper concentration exhibited compact, solid microspheres with average diameters about $2\text{--}4\ \mu\text{m}$. In order to estimate the chemical composition of elements, energy dispersive spectroscopy (EDS) technique employed. The ideal stoichiometry of CZTS exhibits the composition ratio as $\text{Cu}/(\text{Zn} + \text{Sn}) = 1$ and that of $\text{Zn}/\text{Sn} = 1$. The elemental composition and the composition ratio of $\text{Cu}/(\text{Zn} + \text{Sn})$ and Zn/Sn are given in Table 1. It is seen that the CZTS synthesized with 0.01 M copper in the precursor solution exhibited the composition near to the optimum value. Therefore, the sample synthesized using 0.01 M copper concentration (C2) was used for the doctor blade coating of CZTS thin films for counter electrode. Figure 5 shows the SEM image of the doctor blade coated CZTS thin film consists of aggregated particles uniformly distributed over the surface of the FTO substrate. The film exhibits uniform surface and no crack and voids observed on it. The doctor blade coated CZTS thin film further characterized by energy dispersive spectroscopy (EDS) to find chemical composition. From the EDS analysis, the atomic composition of Cu:Zn:Sn:S in the thin film was estimated to be 23.37:13.46:12.81:49.34 respectively. For

high performance CZTS-based solar cell, the optimum composition ratio of $\text{Cu}/(\text{Zn} + \text{Sn})$ and Zn/Sn were reported to be about 0.75–0.95 and 1.1–1.4 respectively [35, 36].

The reaction mechanism involved in the formation of CZTS nanoparticle can be explained based on nucleation, dissolution, and recrystallization mechanism [37]. Thiourea plays important role in the formation metal sulfides. Initially, thiourea in solution acts as a complexing reagent and forms the metal-thiourea ligands. The metal-thiourea ligands serve as metal ions source and regulates the nucleation by the release of metal ions into the solution. Thiourea also acts as a source of sulfur and releases the S_2^{2-} in the solution. On the hydrothermal heating, the released S_2^{2-} combines with the metal ions and precipitate to form metal sulfides [36, 38]. Thus, the gradual release of metal ions from the metal-thiourea ligands and formation S_2^{2-} in the solution can control the nucleation and aggregation of the CZTS nanocrystalites. According to Ostwald ripening theory, because of lower surface free energy large particle grows first and compact and dense microspheres of diameter about 2 to 4 μm gets formed [39].

Figure 6 a–d depicts the SEM images of a dense network of vertically grown one-dimensional TiO₂ nanorod thin film on FTO substrate. From the figure, it seems that the nanorods were grown at 3 h of reaction time, grown without fusing each other and aligned along one dimension with an average diameter of $\sim 150\ \text{nm}$. As the reaction time is increased, initially,

Fig. 4 SEM images of hydrothermal synthesized CZTS nanoparticles using different copper concentrations, 0.005 M Cu (a, b), 0.01 M Cu (c, d), 0.015 M Cu (e, f)



the dense nanorods have formed and then a bunch of uniformly aligned microflowers were observed to be grown on the vertically aligned structures as shown in Fig. 7a–d. Further, the careful observation of Fig. 7a–d shows that the vertically grown dense nanorods still observed on the FTO substrate, which not fully covered with microflowers. Figure 8 a–d represent the intact structures of TiO₂ nanorods covering microflowers all over the vertically grown TiO₂ structures in three-dimensional space. It is observed that the reaction time in the hydrothermal synthesis has a direct impact on the formation of the TiO₂ nanostructures. The lower reaction time

provides enough energy to align the TiO₂ nanorods perpendicular to the FTO substrate. As the reaction time is increased,

Table 1 The chemical composition CZTS nanoparticles synthesized using different copper concentrations

Sample	Cu	Zn	Sn	S	Cu/(Zn + Sn)	Zn/Sn
C1	22.18	13.17	13.10	50.80	0.84	1.00
C2	23.83	13.67	12.89	49.73	0.90	1.06
C3	26.73	12.25	13.18	50.15	1.05	0.92

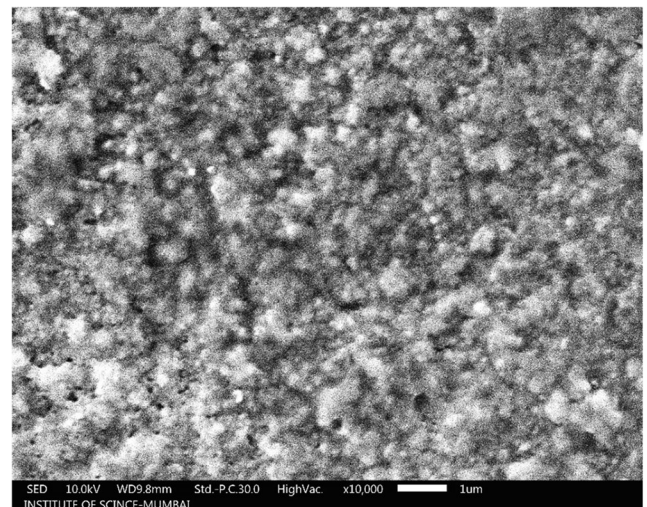
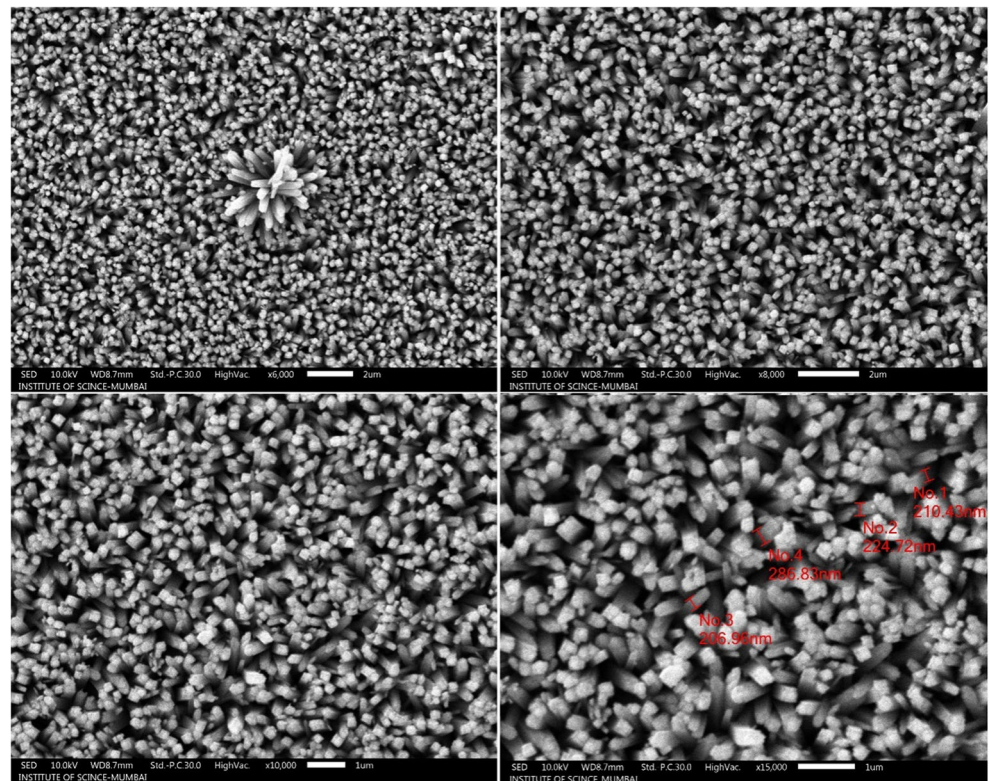


Fig. 5 SEM image of CZTS thin films deposited using the doctor blade coating method

Fig. 6 SEM images of hydrothermal synthesized TiO_2 nanorod deposited at 3 h of reaction time at different resolution



the atom gains enough energy and causes the bundles of microflowers to grow on the vertically grown nanorod

substrate. When reaction time increased to 7 h, many rods like branches grow in three dimensions all over the surface of the 1

Fig. 7 SEM images of hydrothermal synthesized TiO_2 nanorod deposited at 5 h of reaction time at different resolution

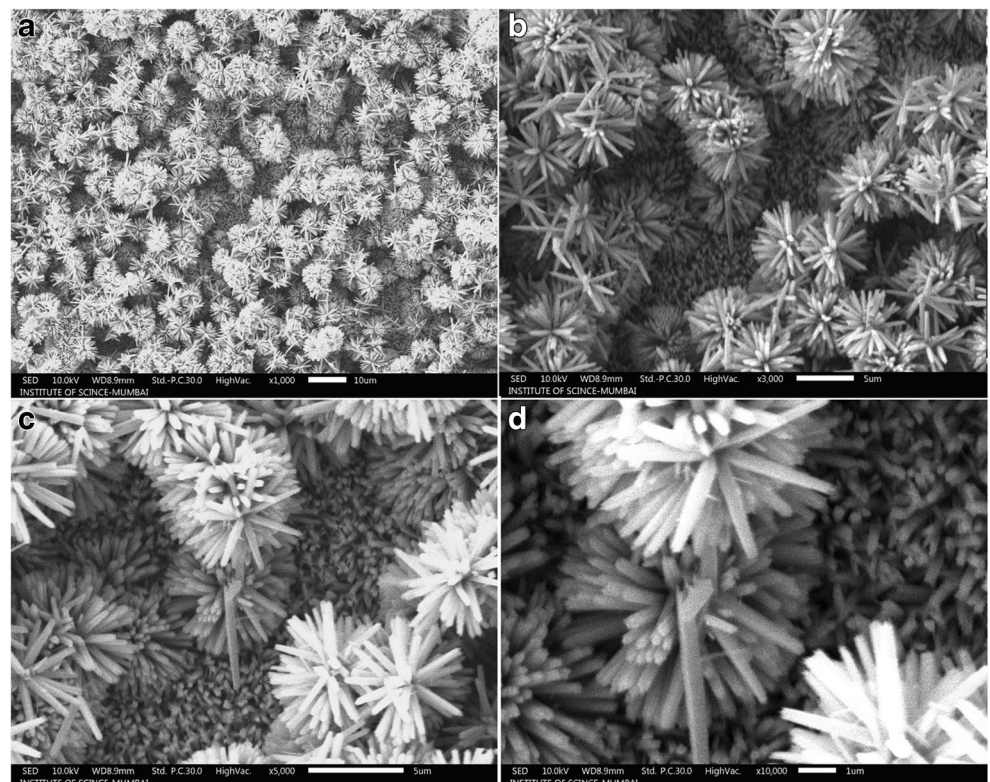
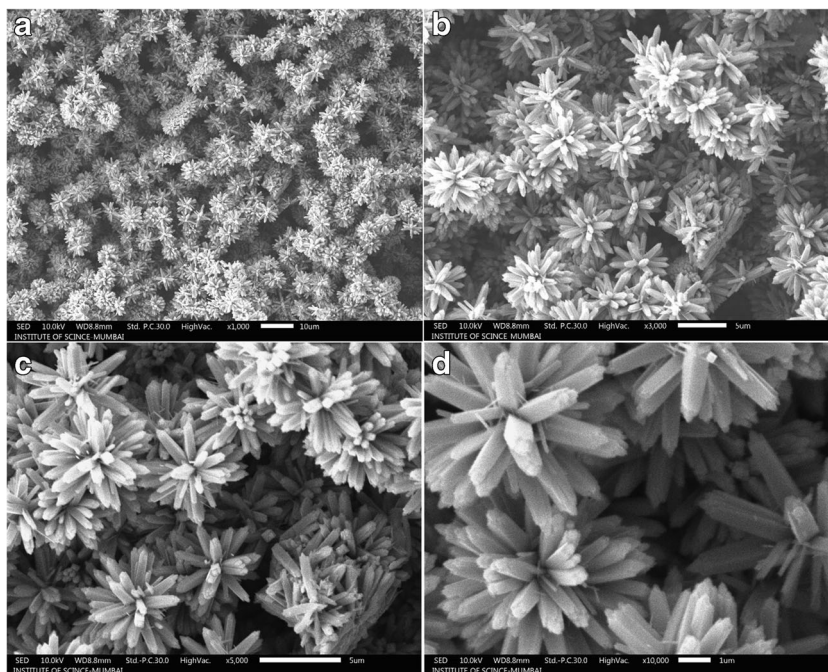


Fig. 8 SEM images of hydrothermal synthesized TiO_2 nanorod deposited at 7 h of reaction time at different resolution



D rods (Fig. 8a–d). Berhe et al. [40] reported similar kind of morphology of TiO_2 thin films deposited using the spin coating technique.

Figure 9 a and b depict the HRTEM images of CZTS nanoparticles and the TiO_2 thin film (sample A3). Figure 6 a showed the lattice fringe pattern of CZTS nanoparticle, indicating the interplanar spacing corresponding to (112) plane is equal to 0.318 nm. Figure 9 b shows the interplanar spacing $d_{(110)} = 0.32$ nm, and $d_{(001)} = 0.29$ nm corresponding to rutile, TiO_2 (110) and TiO_2 (001) planes respectively.

Structural analysis

The structural properties of CZTS nanoparticles synthesized using different copper concentration is shown in Fig. 10a. The

XRD pattern matches well with the diffraction patterns of pure kesterite phase CZTS as in the JCPDS card 52-0868. The XRD pattern of CZTS nanoparticles exhibits strong peaks at 28.4° , 32.36° , 47.2° , and 56.4° can be attributed to (112), (200), (220), and (312) the characteristic peaks of kesterite phase CZTS. There are no additional peaks observed in the XRD patterns of C2 and C3 samples, which indicates the pure CZTS product. However, at a lower Cu concentration, an additional peak of SnS_2 is seen, may be due to nondecomposition of elements in CZTS compound. From the XRD pattern, it is clear that, the intensity of a diffraction peak increased with increasing copper concentration, indicating improved crystalline nature of the sample. The lattice parameters estimated $a = 5.41 \text{ \AA}$, $b = 5.41 \text{ \AA}$, and $c = 10.87 \text{ \AA}$ and matched well with reported values [36]. The average

Fig. 9 a HRTEM image CZTS nanoparticles, b HRTEM image of TiO_2 nanorod thin film

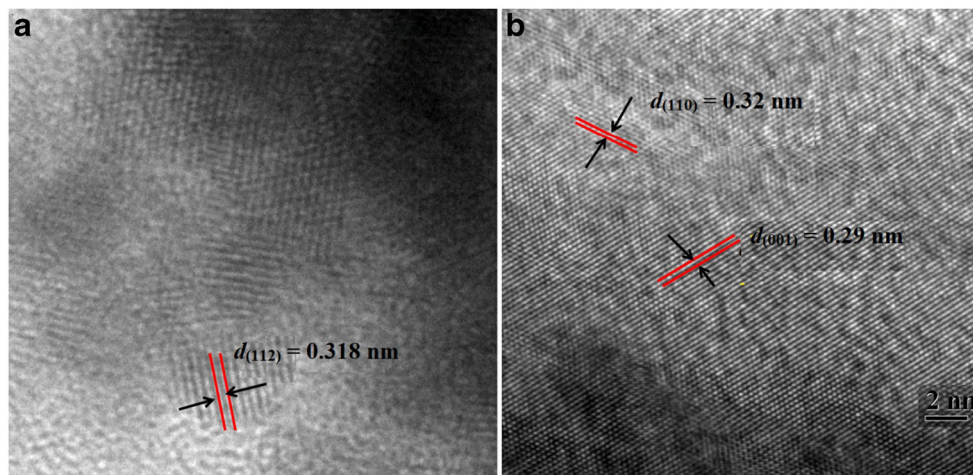
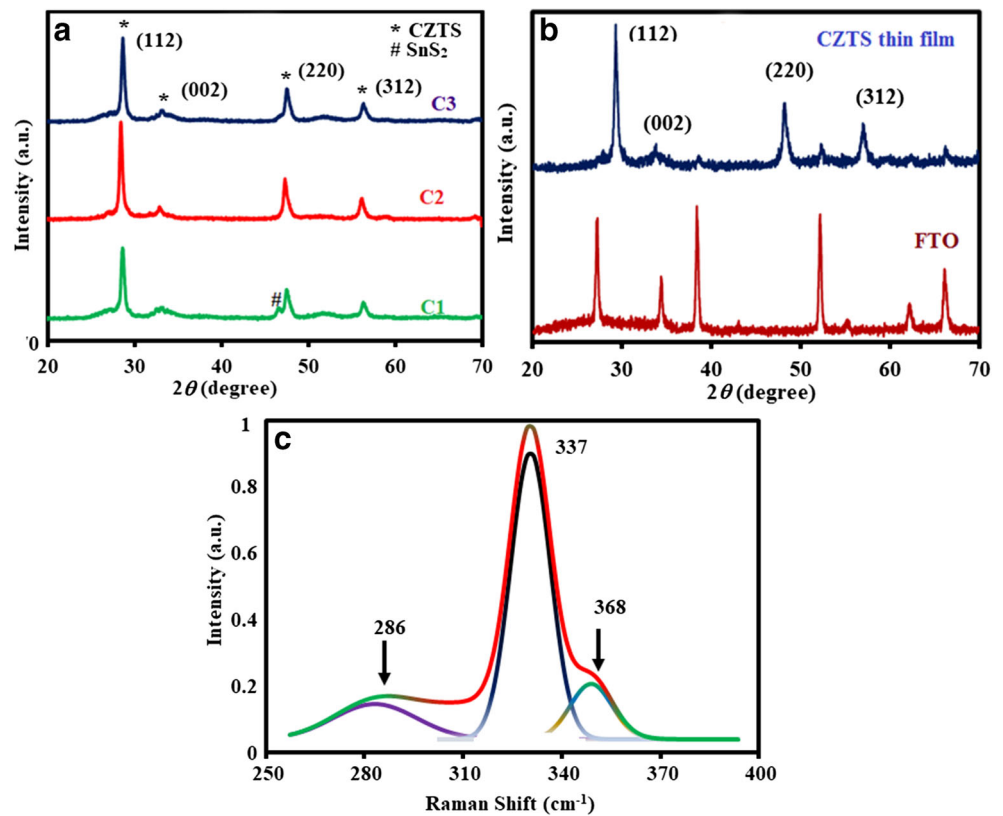


Fig. 10 **a** XRD pattern of CZTS nanoparticles synthesized using 0.005 M Cu (C1), 0.01 M (C2), and 0.015 M (C3) concentrations, **b** XRD pattern of CZTS thin film deposited by doctor blade coating method, and **c** Raman spectra of CZTS thin film



crystal size estimated using Debye–Scherrer formula found to be 16–27 nm. The structural parameters calculated, are summarized in Table 2. Figure 10 b shows the XRD pattern of CZTS thin film deposited using the doctor blade coating technique. The CZTS is a tetrahedral coordinated system, in which sulfur ion bounded with cations Cu, Zn, and Sn and each cation bounded with four sulfur anions. The identification of phase purity of CZTS using XRD is difficult because of possible binary (ZnS, SnS₂, Cu₂S, CuS), ternary (CuSnS₃), and wurtzite phases have a similar XRD pattern as that of CZTS [41, 42]. Therefore, Raman spectroscopy of CZTS thin films recorded and depicted in Fig. 10c. Raman spectra showed three peaks at 287, 338, and 368 cm⁻¹ position, which corresponds to pure phase CZTS as in agreement with earlier reports [43, 44].

Figure 11 depicts the XRD pattern of TiO₂ thin film samples A1, A2, and A3, deposited on FTO substrate. From the XRD patterns, high-crystalline tetragonal rutile phase of TiO₂

(JCPDS card No 01-82-0514) was confirmed. The XRD shows diffraction peaks indexed as (110), (101), (211), and (002), which are the characteristic peak of rutile phase TiO₂ [45]. In the XRD pattern of sample A3 (7 h of reaction time), the (101) and (110) peak intensity is dominant, which indicates (101) and (110) oriented growth of TiO₂ nanorods. The high intensity (101) peak along with (002) in nanorod film suggests that the crystal grown is along [101] direction, parallel to surface of the substrate.

X-ray photoelectron spectroscopic studies of CZTS thin film

The valence states of Cu, Zn, Sn, and S in the CZTS thin film were confirmed by high-resolution XPS analysis. Figure 12 a shows the high-resolution spectrum of Cu 2*p*, two peaks at 932.2 and 952.2 eV appear, indicative of Cu(I) with the energy splitting of 20.0 eV, which is consistent with the standard

Table 2 Structural parameters of CZTS nanoparticle synthesized using various copper concentrations

Sample	FWHM (deg.)	<i>d</i> Spacing (Å)	Lattice parameter (Å)		D–S (nm)
			<i>a</i>	<i>c</i>	
C1	0.490	3.130	5.406	10.873	16.384
C2	0.410	3.130	5.409	10.873	19.278
C3	0.310	3.131	5.406	10.886	27.308

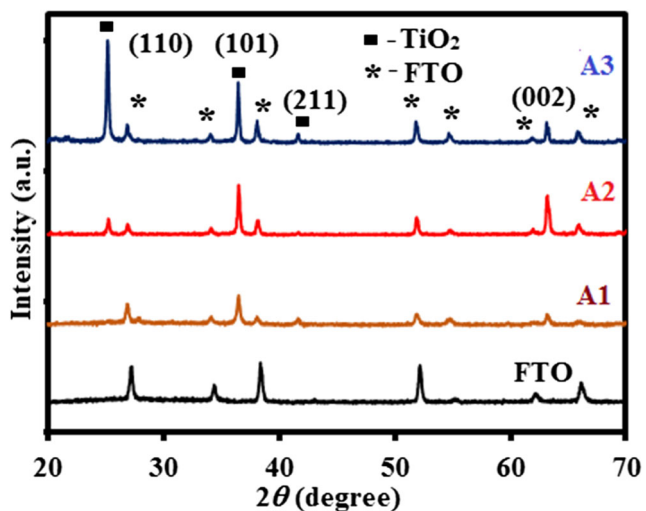


Fig. 11 XRD pattern of TiO₂ nanorod thin films, deposited at 3 h (A1), 5 h (A2), and 7 h (A3) of reaction time

separation of 19.9 eV. The Zn 2*p* peaks located at 1022.2 and 1045.3 eV show a peak separation of 23.1 eV, consistent with the standard splitting of 23.0 eV, suggesting the presence of Zn(II). The presence of Sn(IV) is confirmed by the peak splitting of 8.5 eV of the two peaks located at 486.9 and 495.4 eV. The S 2*p*_{3/2} and 2*p*_{1/2} peaks in the spectra are located at 161.3 and 162.45 eV with a peak splitting of 1.18 eV, which is consistent with the 160–164 eV range expected for the S in

sulfide phases. The oxidation states of the CZTS were found to be 1⁺, 2⁺, 4⁺, and 2⁻ for copper, zinc, tin, and sulfur respectively, and no other valences such as Cu(II) or Sn(II) detected in agreement with previous report [46].

Uv-visible spectroscopy

To study the optical absorption spectra, CZTS nanoparticles were dispersed in ethanol and used for measurement of absorption in the range 350 to 1100 nm at room temperature. The band gap (*E_g*) was estimated by plotting the graph of (*αhν*)² vs (*hν*) and extrapolating with energy axis as shown in Fig. 13a, b. The values of band gap for C1, C2, and C3 samples were estimated to be 1.42, 1.51, and 1.63 eV respectively. The band gap value of C2 sample is near to the optimum value (1.5 eV) required for efficient photovoltaic solar conversion. The observed variation in the band gap value may be due to the compositional variation and the change in crystalline nature with increase of copper concentration. In addition, the disordering between copper and zinc cations is possible in CZTS semiconductors with variation in composition and therefore, there may be variation in the band gap values [47]. Figure 13 b depicts the (*ah*)² vs (*h*) plot of CZTS thin film. Inset of the figure showed the absorption spectra of CZTS thin film. From the plot, it is clear that the CZTS film absorbs most of the light of the visible spectrum. The direct

Fig. 12 High-resolution XPS spectra of CZTS thin film deposited by doctor blade coating method

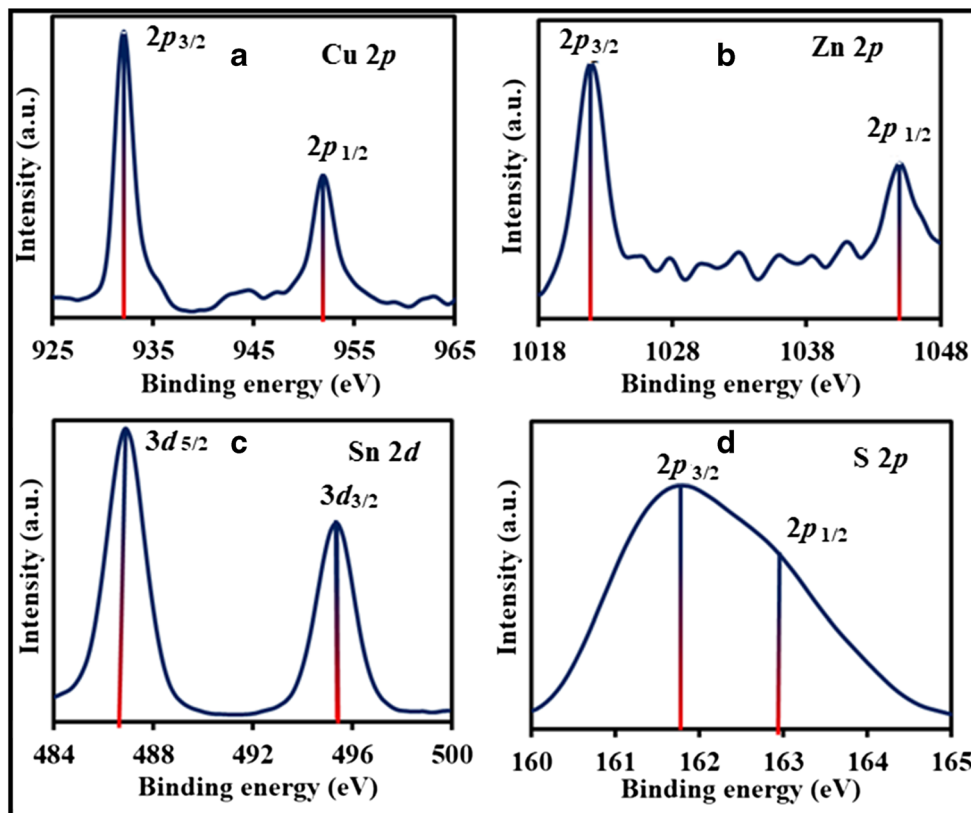
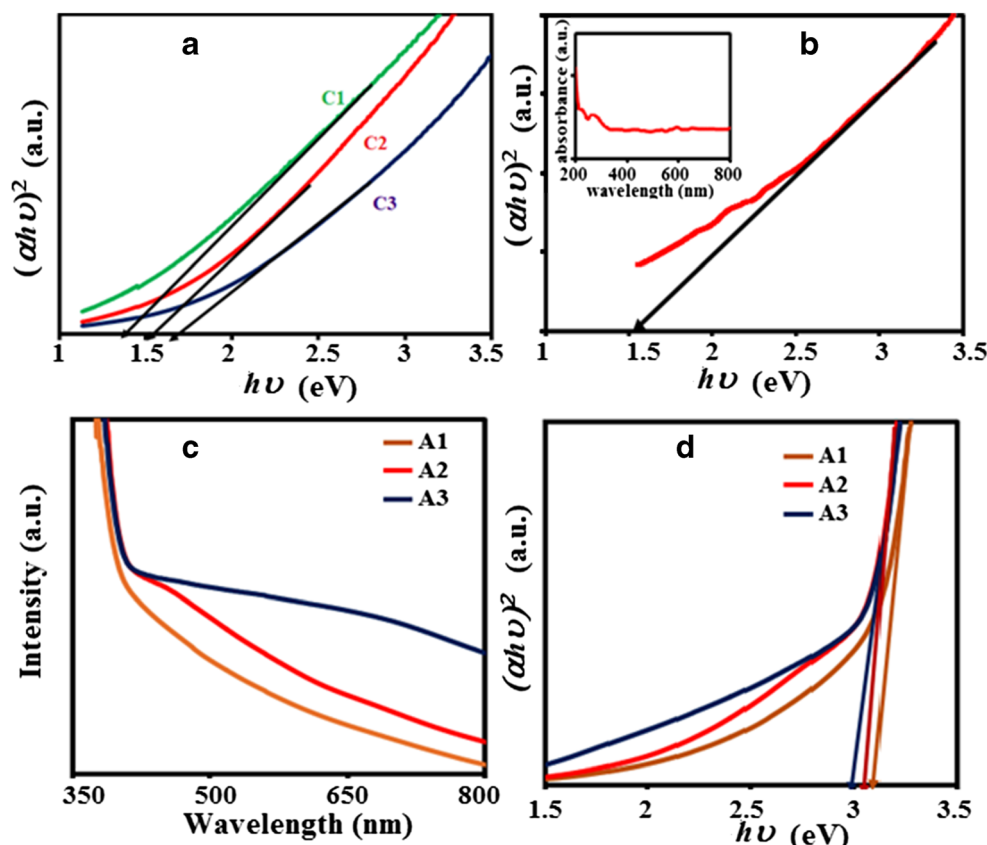


Fig. 13 **a** Plot of $(\alpha h\nu)^2$ vs $(h\nu)$ of CZTS nanoparticles synthesized using 0.005 M Cu (C1), 0.01 M (C2), and 0.015 M (C3) concentrations. **b** Plot of $(\alpha h\nu)^2$ vs $(h\nu)$ of CZTS thin film deposited by doctor blade coating method (C2 sample), inset: Uv-vis spectra for CZTS thin film and **c** Uv-vis spectra of TiO₂ nanorod thin films. **d** Plot of $(\alpha h\nu)^2$ vs $(h\nu)$ of TiO₂ nanorod thin films synthesized by hydrothermal method



optical band gap of CZTS thin film estimated to be about 1.51 eV. The optical absorption spectra and the $(\alpha h\nu)^2$ vs $(h\nu)$ plot for TiO₂ nanostructured thin films deposited using three reaction time are shown in Fig. 13c, d. The estimated direct band gap of TiO₂ nanostructured thin films were estimated to be 2.9, 3.1, and 3.2 eV for 3, 5, and 7 h of reaction times respectively.

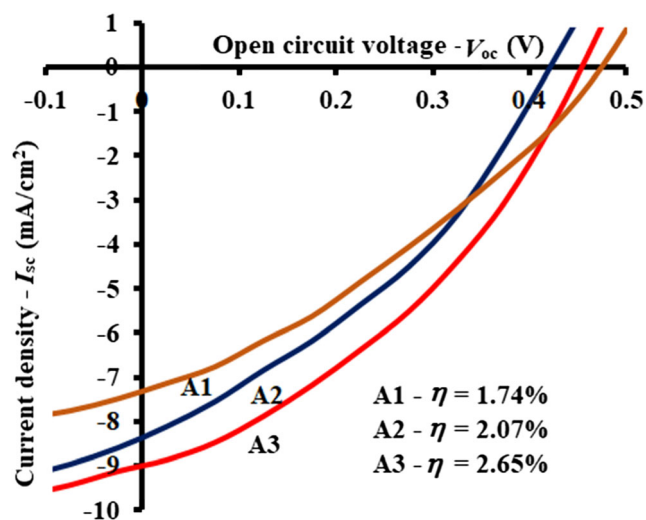


Fig. 14 Current density (I_{sc}) vs open circuit voltage (V_{oc}) characteristics of dye-sensitized solar cell based on CZTS counter electrode

Performance of CZTS counter electrode in DSSCs

Figure 14 depicts the current density vs voltage measurements performed with DSSCs device employing CZTS/FTO counted electrode and N719-TiO₂/FTO working electrodes. The following formulae used to find different solar cell parameters,

$$FF \rightarrow \frac{I_{max} V_{max}}{I_{sc} V_{oc}} \quad (1)$$

$$\eta(\%) \rightarrow \frac{I_{sc} V_{oc}}{P_{in}} \times FF \times 100 \quad (2)$$

where FF is fill factor, η is photoconversion efficiency, I_{max} is maximum current density, V_{max} is maximum voltage, I_{sc} is short circuit current density, and V_{oc} is the open circuit potential. The P_{in} is input power in watt/cm².

Table 3 Solar cell output parameters of dye -ensitized solar cell based on CZTS counter electrode

Sample	I_{sc} (mA/cm ²)	V_{oc} (mV)	FF (%)	η (%)
A1	7.4	0.48	49	1.74
A2	8.3	0.43	58	2.07
A3	9.2	0.46	61	2.65

From the I – V measurement, the short circuit current density (I_{sc}) was observed to be 7.4, 8.3, and 9.2 mA/cm² for A1, A2, and A3 photoanodes respectively. The corresponding open circuit voltage (V_{oc}) were 0.48, 0.43, and 0.46 V respectively. It is observed that the efficiency of the DSSCs increased as the deposition time of the TiO₂ thin film is increased. The photoconversion efficiency (η) of A1, A2, and A3 electrode were 1.74, 2.07, and 2.65%, respectively (device area 0.04 cm²). The electrical measurements performed on DSSCs device are summarized in Table 3. From the observations, it is clear that the TiO₂ nanostructured films with 3D microflower-like morphology facilitate increased light-absorbing ability than 1D nanostructured TiO₂ nanorod films and resulted in higher photo current. Also, due to the relatively large surface area of 3D TiO₂ nanostructures, dye adsorption enhanced and may be the reasons for improved efficiency.

Conclusion

We have successfully synthesized composition controlled kesterite phase CZTS nanoparticle using the hydrothermal method. The CZTS synthesized with 0.01 M copper concentration, exhibits the composition ratio, Cu/(Zn + Sn) = 0.90 and Zn/Sn = 1.05 which is close to the optimum value. Highly oriented 1D and 3D TiO₂ nanostructured thin films successfully deposited using the hydrothermal method on FTO substrate by varying the deposition time. The current-voltage characteristics of solar cell device with CZTS CE and TiO₂ nanostructured thin films as a photoanode, loaded with N719 dye, were measured under AM 1.5 condition. It is observed that, the photoconversion efficiency strongly affected by the morphology of TiO₂ photoanode in CZTS-based dye-sensitized solar cell. The highest efficiency measured was 2.65% with current density of 9.2 mA/cm² and open circuit voltage of 0.46 V for the TiO₂ photoanode with microflower-like structure. The enhanced photoconversion efficiency of DSSCs employing 3D microflower TiO₂ photoanodes and CZTS CEs may be due to the enhanced light-harvesting ability and large surface area of the photoanode. We have demonstrated that CZTS/FTO counter electrodes show the potential to convert the Pt/FTO electrodes to low-cost and earth-abundant element-based counter electrodes.

Acknowledgments Authors are thankful to Director, The Institute of Science, Fort, Mumbai, for the encouragement and providing the necessary facility. Authors are also thankful to INUP.

Funding information This research work is supported by the Department of Science and Technology, India under FIST (SR/FST/PSI-173/2012) program.

References

- Mitzi BD, Gunwan O, Tordov TK, Wang K, Ghuha S (2011) The path towards a high-performance solution-processed kesterite solar cell. *Sol Energy Mater Sol Cells* 95:1421–1436
- Karagiri H, Jimbo K, Yamada S, Kamimura T, Maw SW, Fukano T, Ito T, Motohiro T (2008) Enhanced conversion efficiency of Cu₂ZnSnS₄ – based thin film solar cells by using preferential etching technique. *Appl Phy Express* 1:041201
- Kameyama T, Osaki T, Okazaki K, Shibayama T, Kudo A, Kuwabata S, Torimoto T (2010) Preparation and photoelectrochemical properties of densely immobilized Cu₂ZnSnS₄ thin films. *J Mater Chem* 20:5319–5324
- Ito K, Nakazawa T (1988) Electrical, and optical properties of stan-nite type quaternary semiconductor thin films. *J Appl Phy* 27:2094–2097
- Katagiri H (2005) CuZnSnS thin films solar cells. *Thin Solid Films* 480–481:426–432
- Tordov TK, Tang J, Bag S, Gunwan O, Gokmen T, Zhu Y, Mitzi BD (2013) Beyond 11% efficiency: characteristics of state of the art Cu₂ZnSn(S,Se) solar cells. *Adv Energy Mater* 3:34–38
- Green MA, Hishikawa Y, Dunlop ED, Levi DH, Hohl-Ebinger J, Ho-Baillie AWY (2018) Solar cell efficiency table (version 51). *Prog Photovolt* 26:3–12
- Wang W, Winkler MT, Gunwan O, Gokman T, Tordov TK, Zhu Y, Mitzi BD (2014) Device characteristics of CZTSSe thin film solar cells with 12.6% efficiency. *Adv Energy Mater* 4:1301465
- Chen H, Kou D, Chang Z, Zhou W, Zhou Z, Wu S (2014) Effect of crystallisation of Cu₂ZnSnS_xSe_{4-x} counter electrode on the performance of efficient dye sensitized solar cells. *ACS Appl Mater Interface* 6:20664
- Chen SL, Xu AC, Tao J, Tao HJ, Shen YZ, Zhu LM, Zhu LM, Jiang JJ, Wang T, Pan L (2016) In situ synthesis of two-dimensional leaf-like plate arrays as Pt-free counter electrode for efficient dye sensitized solar cell. *Green Chem* 18(9):2793–2801
- Mali SS, Patil PS, Hong CK (2014) Low cost electrospun crystalline kesterite Cu₂ZnSnS₄ nanofibre counter electrodes for efficient dye sensitized solar cells. *ACS Appl Mater Interface* 6:1688
- Bai B, Kou D, Zho W, Wu S (2015) Applications of quaternary Cu₂ZnSnS₄ quantum dot sensitized solar cells based on hydrolysis approach. *Green Chem* 17:4377–4382
- Riha SC, Parkinson BA, Prieto AL (2011) Compositionally tunable Cu₂ZnSnS_xSe_{4-x} nanocrystals: probing the effect of Se inclusion in mixed chalcogenide thin films. *J Am Chem Soc* 133:15272
- Patel SB, Patel AH, Gohel JV (2018) A novel and cost effective CZTS transport material applied in perovskite solar cells. *J Mater Sci Mater Electron* 20:7677–7687
- Patel SB, Gohel VH (2018) Synthesis of novel counter electrode by combination of mesoporous- microporous CZTS films for enhanced performance of quantum dot sensitized solar cells. *J Mater Sci Mater Electron* 0:1–8
- Chen S, Tao H, She Y, Zhu L, Zeng X, Tao J, Wang T (2015) Facile synthesis of single crystalline sub-micron Cu₂ZnSnS₄ (CZTS) powders using solvothermal treatment. *RSC Adv* 5:6682
- Kong J, Zhu ZJ, Li M, Zhou WH, Yuan SJ, Yao RY, Zho Y, Wu SX (2013) Wurtzite copper zinc tin sulphide as a superior counter electrode material for dye sensitized solar cell. *Nanoscale Res Lett* 8(1): 464
- Varadharajaperumal S, Sripan V, Ganesh R, Hegade G (2017) Morphology controlled n-type TiO₂ and stoichiometry adjusted p-type Cu₂ZnSnS₄ thin films for photovoltaic applications. *Cryst Growth Des* 17:5154–5162
- Dou J, Li Y, Xi F, Ding X, Wei M (2016) Metal organic frame work derived hierarchical porous anatase TiO₂ as a photoanode for dye sensitized solar cell. *Cryst Growth Des* 16:121–125

20. Fan K, Zhang W, Peng T, Chen J, Yang F (2011) Application of TiO₂ fusiform nanorods for dye sensitized solar cells with significant improved efficiency. *J Phys Chem C* 115:17213–17219
21. Zhao K, Pen Z, Zhong X (2016) Charge recombination for high efficiency quantum dot sensitized solar cell. *J Phy Chem Lett* 7: 406–4017
22. Roy P, Kim D, Lee K, Spiecker E, Schmuki P, Bach U, Schmidt-Mende L, Zakeeruddin SM, Kay A, Nazeeruddin MK, Gratzel M, Kim C (2010) TiO₂ nanotubes, and their applications in dye sensitized solar cells. *Nanoscale* 2(1):45–59
23. Shen Q, Qian K, Guan R, Xue J, Zhou L, Liu X, Jia H, Hu L, Xu B (2019) Influence of annealing temperature on microstructure and photoelectric properties of ternary CdSe@CdS@ core shell heterojunctions. *J Solid State Electrochem* 23:2085
24. Shen Q, Xue J, Zhao H, Shao M, Liu X, Jia H (2017) The role of crystalline TiO₂ nanoparticles in enhancing the photocatalytic and photovoltaics properties of CdS nanorods. *J Alloys Compd* 695: 1080
25. Wang K, Gunawan O, Tordov T, Shin B, Chey SJ, Bojarczuk NA, Mitzi D, Guha S (2010) Thermally evaporated Cu₂ZnSnS₄ solar cells. *Appl Phy Lett* 97:143508
26. Seol J, Lee S, Lee J, Nam H, Kim K (2003) Electrical and optical properties of Cu₂ZnSnS₄ thin films prepared by rf magnetron sputtering processes. *Sol Energy Mater Sol Cells* 75:155
27. Williams BA, Smeaton MA, Trejo ND, Francis LF, Aydil ES (2017) Effect of nanocrystals size and carbon on grain growth during annealing of copper zinc thin sulphide nanocrystals coating. *Chem Mater* 29:1676
28. Chan CP, Lam H, Surya C (2010) Preparation of Cu₂ZnSnS₄ films by electrodeposition using ionic liquids. *Sol Energy Mater Sol Cells* 94:209
29. Kamoun N, Bouzouita H, Rezig B (2007) Fabrication and characterization of CZTS thin films deposited by spray pyrolysis method. *Thin Solid Films* 515:5949
30. Chernomordik BD, Ketkat PM, Hunter AK, Beland AE, Deng DD, Aydil ES (2016) Microstructure evolution during selenisation of CZTS colloidal nanocrystals coating. *Chem Mater* 28:1266
31. Yang W, Bob B, Zhou H, Bao L, Chung CH, Sheng-HL HWW, Yang Y (2012) Novel solution processing of high efficiency earth abundant CZTSSe solar cells. *Adv Mater* 24:6323
32. Tordov TK, Bag S, Gukmen O, Zhu Y, Mitzi DB (2013) Beyond 11% efficiency: characteristics of state of art CZTSSe solar cells. *Adv Energy Mater* 3:34
33. Woo K, Kim Y, Moon J (2012) A nontoxic solution processed, earth abundant absorbing layer for thin film solar cell. *Energy Environ Sci* 5:534
34. Wang J, Zhang P, Song X, Gao L (2014) Surfactant free hydrothermal synthesis of CZTS nanocrystals with photocatalytic properties. *RSC Ad* 4:27805
35. Katagiry H, Jimbo K, Maw WS, Oishi K, Yamazaki M, Araki H, Tekeuchi A (2009) Development of CZTS based thin film solar cells. *Thin Sold Films* 517:2455
36. Kishorkumar YB, UdayBhaskar P, Suresh Babu G, Sundara Raja V (2010) Effect of copper salt and thiourea concentration on formation of CZTS thin films by spray pyrolysis method. *Phys Status Solid A* 207:149
37. Yu SH, Shu L, Yang J, Han ZH, Qian YT, Zhang YH (1999) A solvothermal decomposition process for fabrication particle size control of Bi₂S₃ nanowires. *J Mater Res* 14:4157–4162
38. Luo YS, Zhang WD, Dai XJ, Yang Y, Fu SY (2009) Facile synthesis and luminescent properties of novel flower like BaMoO₄ nanostructures by simple hydrothermal route. *J Phys Chem C* 113:4856–4561
39. Roosen AR, Carter WC (1998) Simulation of microstructural evolution: anisotropic growth and coarsening. *Physics A* 261:323
40. Berhe SA, Nag S, Molinets Z, Youngblood WJ (2013) Influence of seeding and bath conditions in hydrothermal growth of very thin (~ 20 nm) single crystalline rutile TiO₂ nanorod films. *ACS Appl Mater Interface* 5:1181–1185
41. Kong J, Zhou Z, Li M, Zhou WH, Yuan SJ, Yao R, Zhao Y, Wu S (2013) Wurtzite copper zinc tin sulphide as a superior counter electrode for dye sensitized solar cells. *Nanoscale Res Let* 8:464
42. Li M, Zhou WH, Guo J, Zhou YL, Hou ZL, Jiao J, Zhou ZJ, Du ZL, Wu S (2012) Synthesis of pure metastable wurtzite CZTS nanocrystals by one pot method. *J Phys Chem C* 116(50):26507
43. Jin WC, Agus I, Park SJ, Kim W, Yoon S, Min BK (2013) Synthesis of Cu₂ZnSnS₄ thin films by a precursor solution paste for thin film solar cell application. *ACS Appl Mater Interface* 5:4162
44. Zou C, Zhang LJ, Lin DS, Yang Y, Li Q, Xu XJ, Chen X, Huang SM (2011) Facile synthesis of Cu₂ZnSnS₄ nanocrystals. *Crystengcomm* 13:3310
45. Ghoderao KP, Jambhale SN, Kale RB (2018) Influence of reaction temperature and on hydrothermally grown TiO₂ nanorods and their performance in dye sensitised solar cell. *Superlattice and microstructures* 124:121–130
46. Yin X, Tang C, Chem M, Adms S, Wang H, Gong H (2013) Hierarchical porous Cu₂ZnSnS₄ films for high capacity reversible lithium storage application. *J Mater Chem A* 48:9162–9164
47. Fan FJ, Wu L, Gong M, Liu G, Wang YX, Yu SH, Chen S, Wang LW, Gong XG (2013) Composition and band gap tunable synthesis wurtzite-derived Cu₂ZnSnS_(1-x)Se_{x4} nanocrystals: theoretical and experimental insight. *ACS Nano* 7:1454

Part of the reported work (characterization) was carried out at IITBNF, IITB under INUP which is sponsored by deity, MCIT, Government of India.

Publisher's note Springer Nature remains neutral with regard to jurisdictional claims in published maps and institutional affiliations.